Two distinct effects of PIP_2 underlie auxiliary subunit-dependent modulation of Slo1 BK channels

Yutao Tian,[1] Florian Ullrich,[2] Rong Xu,[1] Stefan H. Heinemann,[2] Shangwei Hou,[3] and Toshinori Hoshi[1]

[1]Department of Physiology, University of Pennsylvania, Philadelphia, PA 19104
[2]Department of Biophysics, Center for Molecular Biomedicine, Friedrich Schiller University Jena and Jena University Hospital, D-07745 Jena, Germany
[3]Key Laboratory of Systems Biomedicine, Shanghai Center for Systems Biomedicine, Shanghai Jiao Tong University, Shanghai 200240, China

Phosphatidylinositol 4,5-bisphosphate (PIP_2) plays a critical role in modulating the function of numerous ion channels, including large-conductance Ca^{2+}- and voltage-dependent K^+ (BK, Slo1) channels. Slo1 BK channel complexes include four pore-forming Slo1 (α) subunits as well as various regulatory auxiliary subunits (β and γ) that are expressed in different tissues. We examined the molecular and biophysical mechanisms underlying the effects of brain-derived PIP_2 on human Slo1 BK channel complexes with different subunit compositions that were heterologously expressed in human embryonic kidney cells. PIP_2 inhibited macroscopic currents through Slo1 channels without auxiliary subunits and through Slo1 + γ1 complexes. In contrast, PIP_2 markedly increased macroscopic currents through Slo1 + β1 and Slo1 + β4 channel complexes and failed to alter macroscopic currents through Slo1 + β2 and Slo1 + β2 Δ2–19 channel complexes. Results obtained at various membrane potentials and divalent cation concentrations suggest that PIP_2 promotes opening of the ion conduction gate in all channel types, regardless of the specific subunit composition. However, in the absence of β subunits positioned near the voltage-sensor domains (VSDs), as in Slo1 and probably Slo1 + γ1, PIP_2 augments the negative surface charge on the cytoplasmic side of the membrane, thereby shifting the voltage dependence of VSD-mediated activation in the positive direction. When β1 or β4 subunits occupy the space surrounding the VSDs, only the stimulatory effect of PIP_2 is evident. The subunit compositions of native Slo1 BK channels differ in various cell types; thus, PIP_2 may exert distinct tissue- and divalent cation–dependent modulatory influences.

INTRODUCTION

Large-conductance Ca^{2+}- and voltage-dependent K^+ (BK, Slo1) channels are broadly expressed in numerous cell types and regulate many critical physiological processes including neuronal excitability, synaptic transmission, and vascular tone (Salkoff et al., 2006; Hoshi et al., 2013a). To serve these diverse roles, Slo1 BK channels are equipped with multiple mechanisms to increase their functional versatility. For example, Slo1 BK channels are allosterically activated by both intracellular Ca^{2+} and membrane depolarization (Horrigan and Aldrich, 2002; Hoshi et al., 2013a). Furthermore, native BK channel complexes include four pore-forming Slo1 (α) subunits as well as auxiliary subunits in a tissue-dependent manner (Knaus et al., 1994b; Wallner et al., 1999; Xia et al., 1999; Brenner et al., 2000; Uebele et al., 2000; Yan and Aldrich, 2010, 2012; Yang et al., 2011). Two vertebrate families of Slo1 auxiliary subunits are known: the β-subunit family with four members (β1–β4) (Knaus et al., 1994b; Wallner et al., 1999; Xia et al., 1999; Brenner et al., 2000; Uebele et al., 2000) and the γ-subunit family with multiple members including leucine-rich repeat-containing (LRRC) protein 26 or γ1 (Yan and Aldrich, 2010, 2012; Yang et al., 2011). Both β and γ subunits are expressed in a tissue-specific manner to fine-tune the properties of the resulting channel complexes. For example, β1-containing BK channels are found abundantly in vascular smooth muscle cells (Knaus et al., 1994b) and promote muscle relaxation (Nelson and Bonev, 2004). β4-containing BK channels are found readily in the nervous system (Behrens et al., 2000; Brenner et al., 2000). Slo1 BK complexes with γ1 are found in testis-related cells and other cell types (Yang et al., 2011; Almassy and Begenisich, 2012; Evanson et al., 2014).

Correspondence to Yutao Tian: yttian1983@gmail.com; or Toshinori Hoshi: hoshi@hoshi.org

F. Ullrich's present address is Leibniz Institute for Molecular Pharmacology and Max Delbrück Center for Molecular Medicine, D-13125 Berlin, Germany.

Abbreviations used in this paper: BK, large-conductance Ca^{2+}- and voltage-dependent K^+; DHA, docosahexaenoic acid; GR, gating ring; HA model, Horrigan and Aldrich model; LRRC, leucine-rich repeat-containing; PIP_2, phosphatidylinositol 4,5-bisphosphate; P_o, open probability; VSD, voltage-sensor domain.

The Rockefeller University Press $30.00
J. Gen. Physiol. Vol. 145 No. 4 331–343
www.jgp.org/cgi/doi/10.1085/jgp.201511363

Structurally, β subunits contain two transmembrane segments, TM1 and TM2, connected by an extracellular linker, placing the N and C termini on the intracellular side (Knaus et al., 1994a,b). Each β subunit is located most probably between two adjacent voltage-sensor domains (VSDs) (Wu et al., 2009, 2013; Morera et al., 2012; Liu et al., 2015), and up to four β subunits may be found within a tetrameric Slo1 complex (Knaus et al., 1994b; Wang et al., 2002). In contrast with β subunits with two transmembrane segments, γ subunits are processed to contain only one transmembrane segment with its long N-terminal LRRC segment facing the extracellular side (Yan and Aldrich, 2010).

To further increase the functional versatility, gating of Slo1 BK channels is modulated by various signaling molecules, such as CO, H^+, heme, and lipids (Hou et al., 2009). Modulation of Slo1 BK currents by a wide variety of lipid species, including free fatty acids, epoxyeicosatrienoic acids, cholesterol, and phosphoinositides, has been reported (Dopico and Bukiya, 2014). Among them, phosphatidylinositol 4,5-bisphosphate (PtdIns(4,5)P_2, herein referred to as PIP_2) is found in the inner leaflet of the plasma membrane and plays many cell signaling roles (Balla, 2013). Structurally, PIP_2 possesses a negatively charged inositol head group and two nonpolar fatty acid tails, commonly stearic (C18:0) and arachidonic (C20:4) forms (Balla, 2013). Functionally, PIP_2 directly regulates a variety of ion channels with a diverse range of affinities, typically by binding to positively charged regions of the proteins located near the membrane (Gamper and Shapiro, 2007; Suh and Hille, 2008; Hansen et al., 2011). In many channels, the binding of PIP_2 acts to maintain their functionalities; this is well illustrated in so-called "rundown" phenomena often caused by depletion of PIP_2, in which PIP_2 essentially acts as a functionally necessary cofactor (Balla, 2013). More complex modulatory phenomena by PIP_2 have been also reported. For example, CNG channels in rod photoreceptors are inhibited by PIP_2, whereas CNG channels in olfactory receptors are PIP_2 insensitive (Womack et al., 2000). Furthermore, PIP_2 may exert both excitatory and inhibitory influences in the same channels through multiple interaction sites, as shown in capsaicin-sensitive TRPV1 and hyperpolarization-activated cation channels (Womack et al., 2000; Pian et al., 2006; Flynn and Zagotta, 2011; Hansen et al., 2011).

In Slo1 BK channels, the application of exogenous PIP_2 increases open probability (P_o) (Rittenhouse, 2008; Vaithianathan et al., 2008; Tang et al., 2014) and also the number of functional channels available to open after enzymatic depletion of bound PIP_2 (Tang et al., 2014). Exactly which aspect of gating of the Slo1 channel, often described by the multi-tier allosteric model of Horrigan and Aldrich (2002) (HA model), is altered by PIP_2 to increase P_o remains unclear. PIP_2 has been suggested to interact with the S6-RCK1 linker region of Slo1 (^{329}RKK^{331} using the human Slo1 numbering) (Vaithianathan et al., 2008) and also with a segment near the RCK1 Ca^{2+} sensor area ("^{366}KDRDD^{370} loop") in the cytoplasmic gating ring (GR) domain (Tang et al., 2014).

We describe here functional impacts of the application of brain-derived PIP_2 on the gating of heterologously expressed human Slo1 BK channels with different auxiliary subunit compositions. We show that the application of PIP_2 can enhance or diminish currents through Slo1 BK channels depending on the subunit composition, and describe two distinct biophysical mechanisms that account for this subunit composition–dependent modulation by PIP_2 based on the probable location of the auxiliary subunits within the Slo1 BK channel complex.

MATERIALS AND METHODS

Channel expression

Human Slo1 (KCNMA1; GenBank accession no. AAB65837) and their auxiliary subunits β1 (KCNMB1; RefSeq accession no. NP_004128), β2 (KCNMB2; RefSeq accession no. NP_852006), β4 (KCNMB4; GenBank accession no. AAF69805), and LRRC26 (RefSeq accession no. NP_001013675) were transiently expressed in human embryonic kidney cells, as described previously (Hoshi et al., 2013c). The cells were maintained in Dulbecco's modified Eagle's medium (ATCC), 10% FBS (ATCC), 1% penicillin/streptomycin at 37°C, and 5% CO_2. For those experiments involving coexpression of Slo1 and an auxiliary subunit, the DNA weight ratio in transfection was typically 1:1. Functional coassembly with the auxiliary subunits in each patch was verified by observing the characteristically altered gating properties conferred, such as slowing of the activation and deactivation kinetics (Hoshi et al., 2013b) (see Fig. S5). Electrophysiological characteristics of ionic currents recorded from cells transfected with Slo1 and various auxiliary subunit DNAs together were clearly different from those of Slo1 currents without any auxiliary subunit, suggesting adequate coassembly of Slo1 and the auxiliary subunits.

To express Slo1 in *Xenopus laevis* oocytes, human Slo1 in pCI-neo was linearized with NotI and the RNA was prepared using the T7 RNA polymerase. Surplus oocytes, which were harvested according to an institutionally approved protocol and which would have been otherwise wasted, were obtained from the laboratory of Zhe Lu (University of Pennsylvania, Philadelphia, PA) and injected with the Slo1 RNA.

Electrophysiology and analysis

Currents were recorded using the inside-out patch-clamp method with an AxoPatch 200A or 200B amplifier (Molecular Devices). Borosilicate electrodes coated with dental wax had a typical initial input resistance of 0.9–2 MΩ, and ∼60% of the input resistance was electronically compensated. Tight seals were formed as quickly as possible without much negative pressure; only the results from the seals formed within a few seconds were analyzed. The output of the amplifier was filtered through its built-in 10-kHz filter, digitized, and analyzed as described using routines running in IGOR Pro (WaveMetrics) (Horrigan et al., 2005). The external solution typically contained (mM): 140 KCl, 2 $MgCl_2$, and 10 HEPES, pH 7.2 with NMDG. The internal solution without Ca^{2+} contained (mM): 140 KCl, 11 EGTA, and 10 HEPES, pH 7.2 with NMDG. The solution with different concentrations of Ca^{2+} was as in Horrigan et al. (2005). For each channel type, voltage-pulse durations were adjusted to allow for steady-state measurements. Normalized conductance (G/G_{max})–voltage curves were constructed from extrapolated instantaneous tail current

amplitudes. The voltage dependence in each dataset was fitted by a Boltzmann-type equation as described previously (Horrigan et al., 2005) and characterized by two parameters: the half-activation voltage ($V_{0.5}$) and the number of equivalent charges (Q_{app}) (Hoshi et al., 2013b,c). PIP_2 was applied typically 6–8 min after patch excision after ensuring that the ionic currents were stable in size and kinetics. In the virtual absence of Ca^{2+}, confounding associated with rundown was minimal (Zhang et al., 2006). In each patch, changes in voltage dependence of activation by PIP_2 were described by changes in half-activation voltage ($\Delta V_{0.5}$) and the fractional change in apparent charge movement (Q_{app} ratio). Estimated equation parameter values are presented as mean ± 95% confidence interval as implemented in IGOR Pro. Kinetics of Slo1 currents were characterized by single exponentials. Estimation of P_o from single-channel openings was performed using all-point amplitude histograms (Horrigan et al., 2005). In each patch, the number of functional channels present was estimated from the peak macroscopic current size at a very positive voltage (e.g., 220 mV) and the unitary current size.

Reagents

PIP_2 purified from the bovine brain was obtained from Sigma-Aldrich, and diC8 PIP_2 was obtained from Echelon Biosciences. Brain PIP_2 was dissolved in water (3 mM) by sonication in cold water bath and vigorous vortexing. The stock solution was stored at −20°C and diluted to the final concentrations immediately before experiments by vigorous vortexing.

Statistics

The numbers of independent measurements are indicated in the figures. Statistical results in the text are presented as mean ± SEM (n), where n is the number of independent measurements. The Mann–Whitney or Wilcoxon test with an α level of 0.05, which was corrected for multiple comparisons using the Bonferroni method when appropriate, was used to evaluate statistical significance.

Online supplemental material

The concentration dependence and the slow reversibility of brain-derived PIP_2 are illustrated in Fig. S1. The results obtained from Slo1 channels expressed in *Xenopus* oocytes are shown in Fig. S2. We show that diC8 PIP_2 is less effective than brain-derived PIP_2 in Fig. S3. The nonessential role of the Ca^{2+} sensors of the Slo1 channel is presented in Figs. S4 and S6. Adequate coassembly of Slo1 mutants and β1/β4 are illustrated in Fig. S5. The online supplemental material is available at http://www.jgp.org/cgi/content/full/jgp.201511363/DC1.

RESULTS

Subunit-dependent regulation by brain-derived PIP_2

We systematically compared the effects of the application of brain-derived PIP_2 to the cytoplasmic side of Slo1 BK channel complexes with different subunit compositions:

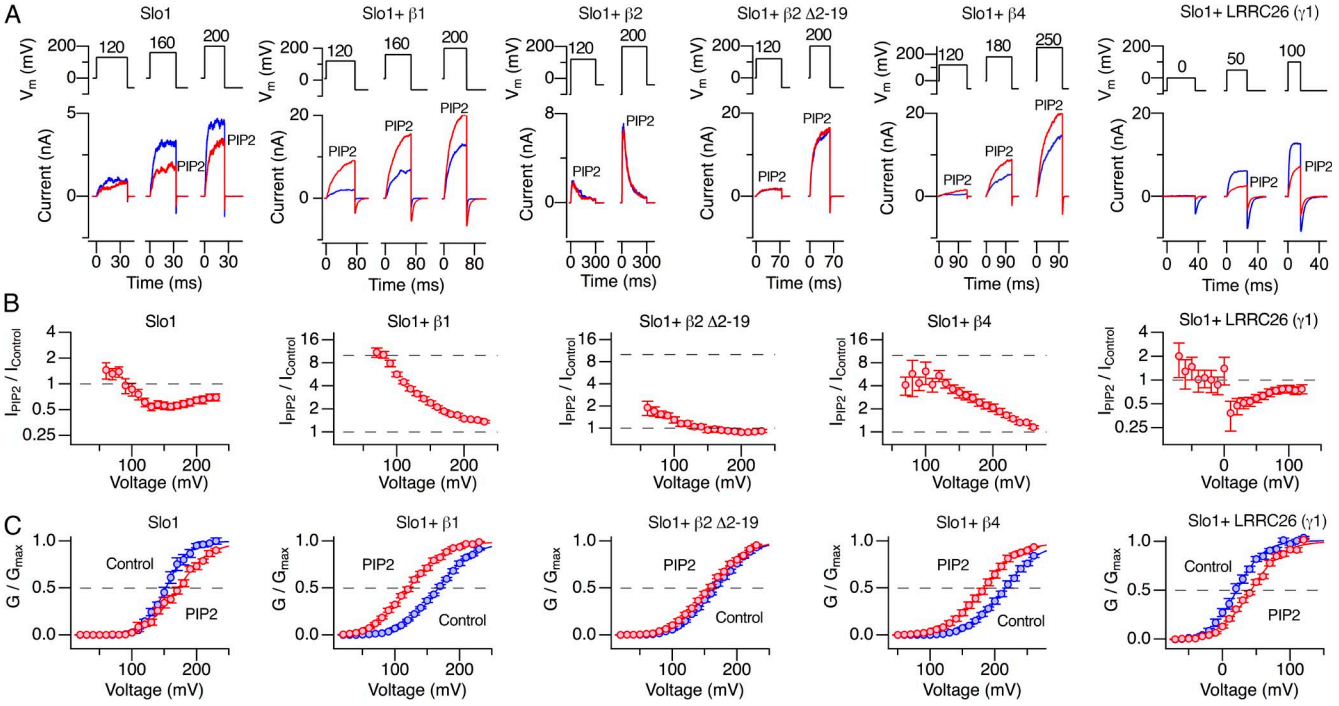

Figure 1. Effects of PIP_2 on Slo1 complexes with different subunit compositions. (A) Illustrative currents through Slo1, Slo1 + β1, Slo1 + β2, Slo1 + β2 Δ2–19, Slo1 + β4, and Slo1 + LRRC26 (γ1). In each panel, currents before (blue) and after (red) the application of 10 µM PIP_2 to the cytoplasmic side recorded without Ca^{2+} are shown. Pulses were applied from 0 mV every 3 s except for Slo1 + β2, which was stimulated every 10 s. For Slo1 + β2, 1-s prepulses to −100 mV preceded depolarization pulses. For Slo1 + LRRC26 (γ1), the holding voltage was −80 mV. (B) Fractional changes in peak outward currents in Slo1, Slo1 + β1, Slo1 + β2, Slo1 + β2 Δ2–19, Slo1 + β4, and Slo1 + LRRC26 (γ1). (C) Normalized conductance (G-V) curves before (blue) and after (red) the application of 10 µM PIP_2 in the channels indicated. The smooth curves are Boltzmann fits to the results with: Slo1, $V_{0.5}$ = 154.5 ± 3.1 mV and Q_{app} = 1.33 ± 0.04 (Control), and 170.1 ± 2.7 mV and 1.18 ± 0.05 (PIP_2); Slo1 + β1, $V_{0.5}$ = 167.8 ± 2.0 mV and Q_{app} = 0.92 ± 0.02 (Control), and 122.3 ± 2.8 mV and 0.95 ± 0.03 (PIP_2); Slo1 + β2 Δ2–19, $V_{0.5}$ = 163.9 ± 3.0 mV and Q_{app} = 0.98 ± 0.02 (Control), and 158.6 ± 2.4 mV and 0.92 ± 0.02 (PIP_2); Slo1 + β4, $V_{0.5}$ = 217.2 ± 3.2 mV and Q_{app} = 0.99 ± 0.03 (Control), and 183.2 ± 4.0 mV and 1.00 ± 0.03 (PIP_2); and Slo1 + LRRC26 (γ1), $V_{0.5}$ = 20.9 ± 3.5 mV and Q_{app} = 1.38 ± 0.06 (Control), and 42.3 ± 1.8 mV and 1.09 ± 0.04 (PIP_2); n = 9–18. Error bars represent mean ± SEM.

Slo1 without any auxiliary subunit (hereafter referred to as Slo1), Slo1 + β1, Slo1 + β2, Slo1 + β4, and Slo1 + LRRC26 (γ1) (Knaus et al., 1994b; Wallner et al., 1999; Xia et al., 1999; Brenner et al., 2000; Uebele et al., 2000; Yan and Aldrich, 2010, 2012; Yang et al., 2011). We also examined the effect of PIP_2 on Slo1 + β2 with a deletion in the β2 N terminus (Δ2–19) to remove inactivation (Wallner et al., 1999; Uebele et al., 2000; Xia et al., 2003). Representative macroscopic ionic currents recorded from the aforementioned channel complexes before and after application of 10 µM PIP_2 in the virtual absence of Ca^{2+} to the intracellular side are shown in Fig. 1 A. This concentration was a functionally saturating "bulk" concentration of PIP_2; 30 µM caused no further change (Fig. S1). PIP_2 clearly decreased macroscopic currents through Slo1 and Slo1 + γ1 but increased macroscopic currents through Slo1 + β1 and Slo1 + β4 (Fig. 1, A and B). PIP_2 had no appreciable effect on Slo1 + β2 Δ2–19 (Fig. 1, A and B). The differential impacts of PIP_2 on these channel types were also evident in their voltage dependence of normalized conductance (G/G_{max}) curves (G-V curves) before and after the application of PIP_2 (Fig. 1 C). In Slo1, PIP_2 shifted the half-activation voltage ($V_{0.5}$) of G-V to the positive direction by 15.6 ± 2.6 mV (9). In contrast, in Slo1 + β1 and Slo1 + β4, PIP_2 moved the G-V curves to the negative direction ($\Delta V_{0.5}$ = −45.5 ± 2.1 mV [18] and −33.9 ± 2.8 mV [16], respectively). Slo1 + β2 Δ2–19 showed no change in $V_{0.5}$ ($\Delta V_{0.5}$ = −5.3 ± 2.1 mV [18]), whereas Slo1 + γ1 showed a positive shift of $V_{0.5}$ ($\Delta V_{0.5}$ = 21.4 ± 3.3 mV [9]), similar to that observed in Slo1. These effects of PIP_2 were very poorly reversible by wash (Fig. S1, A and C).

PIP_2 also altered the ionic current kinetics in a subunit composition–dependent manner (Fig. 2). The current enhancement by PIP_2 observed in Slo1 + β1 and Slo1 + β4 was accompanied by deceleration of the kinetics at the voltages where G/G_{max} is less than ∼0.5 and acceleration of the kinetics at more positive voltages. In Slo1 and Slo1 + γ1, in which the currents were inhibited, PIP_2 preferentially slowed the kinetics at the voltages where G/G_{max} is greater than ∼0.5.

Next, we will focus on the following three subunit-dependent phenomena caused by brain-derived PIP_2: (1) macroscopic current inhibition in Slo1 but current enhancement in Slo1 + β1 and Slo1 + β4 (Fig. 1, A and B), (2) macroscopic current enhancement in Slo1 + β1 and Slo1 + β4 but no marked effect in Slo1 + β2 Δ2–19 (Fig. 1, A and B), and (3) the molecular loci responsible for the effects of PIP_2 on Slo1 and Slo1 + β1.

Slo1 versus Slo1 + β1

In Slo1, PIP_2 shifts its $V_{0.5}$ to the positive direction and decreases macroscopic currents at voltages >120 mV (Fig. 1 B). In contrast, in Slo1 + β1, PIP_2 shifts its $V_{0.5}$ to the negative direction and enhances macroscopic currents (Fig. 1 B). A similar inhibitory effect of PIP_2 was

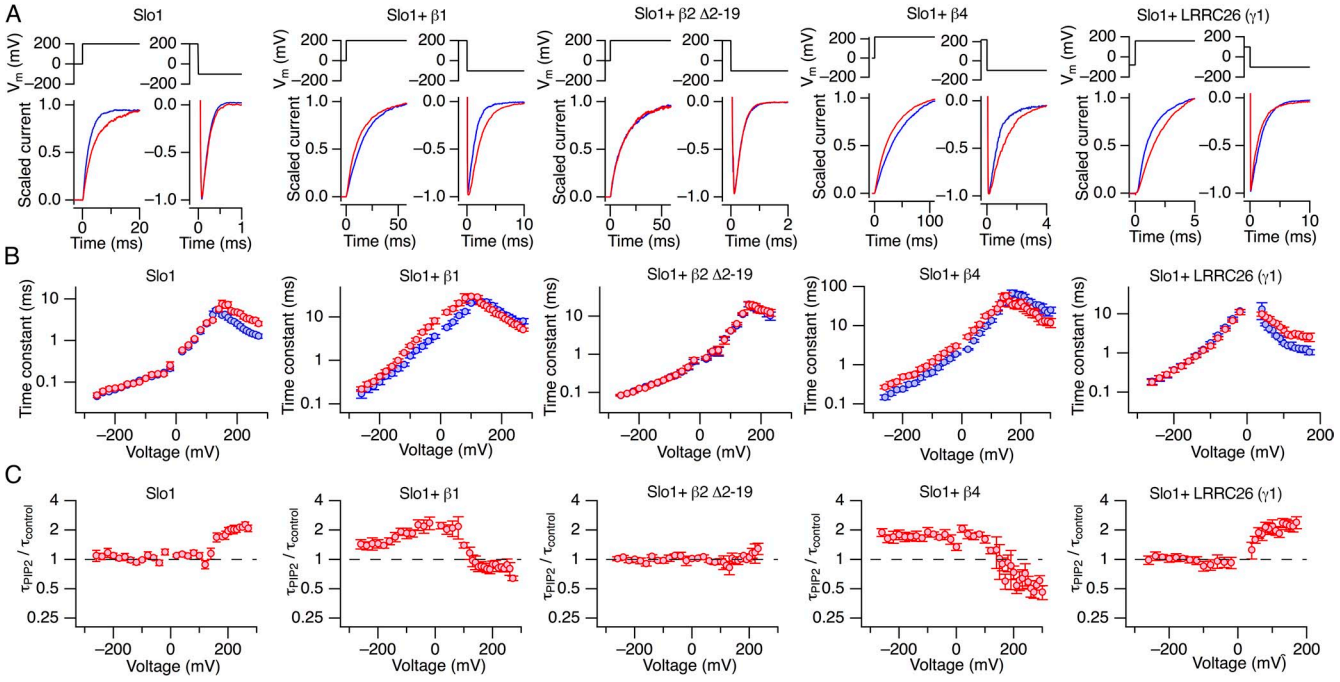

Figure 2. Changes in kinetics of ionic currents by PIP_2. (A) Scaled representative currents through Slo1, Slo1 + β1, Slo1 + β2 Δ2–19, Slo1 + β4, and Slo1 + LRRC26 (γ1) before (blue) and after (red) the application of 10 µM PIP_2. (B) Time constant (τ) of ionic currents at different voltages before (blue) and after (red) the application of 10 µM PIP_2 in the channels indicated. (C) Fractional changes in time constant of ionic currents by 10 µM PIP_2. All results shown were obtained without Ca^{2+}; n = 6 to 12. Error bars represent mean ± SEM.

observed using Slo1 channels heterologously expressed in *Xenopus* oocytes (Fig. S2). The application of diC8 PIP_2, a more water-soluble PIP_2 analogue with short eight-carbon tails, produced no effect on Slo1 but increased currents through Slo1 + β1, albeit to a lesser extent (Fig. S3), suggesting that the long tail groups of brain-derived PIP_2 contribute to its action on Slo1 and Slo1 + β1 channels, as seen in an earlier study (Vaithianathan et al., 2008).

Gating of the Slo1 channel is allosteric, encompassing three gating tiers, the ion conduction gate, VSDs, and divalent cation sensors, as summarized in the HA model (Horrigan and Aldrich, 2002). The three allosteric tiers can be studied in relative isolation by manipulating membrane potential and intracellular Ca^{2+} concentration ($[Ca^{2+}]_i$) (Horrigan and Aldrich, 2002). In the absence of Ca^{2+} at very negative voltages where the VSDs are mostly at rest, PIP_2 increased P_o in both Slo1 (Fig. 3, A and C) and Slo1 + β1 (Fig. 3, B and C), and the fractional increases were indistinguishable between the two channel types (P = 0.955; Fig. 3 D), despite the contrasting effects at more positive voltages where VSD activation and G/G_{max} are appreciable. P_o at negative voltages without Ca^{2+} primarily reflects the weakly voltage-dependent equilibrium of the ion conduction gate (L_0 in the HA model). According to the HA model, an increase in the value of L_0 as suggested by our single-channel P_o measurements predicts a negative shift in $V_{0.5}$. For Slo1 + β1, this prediction is born out; however, for Slo1, whose macroscopic currents are inhibited by PIP_2, the prediction obviously does not hold. We postulated that the inhibitory effect of PIP_2 on Slo1 at positive voltages where VSD activation and G/G_{max} are noticeable may represent a separate phenomenon superimposed on the common stimulatory effect readily observed at negative voltages without Ca^{2+} in both Slo1 and Slo1 + β1.

Membrane phospholipids with charged head groups are capable of altering functions of voltage-gated ion channels by directly interacting with the VSD and/or by influencing the membrane surface charge (Ramu et al., 2006; Xu et al., 2008; Hite et al., 2014). We hypothesized that the application of PIP_2 with the net charge of about −4 (Wang et al., 2014) to the intracellular side augments the negative surface charge on the intracellular membrane surface, and that this enhanced negative surface charge may underlie the inhibitory influence of PIP_2 on the macroscopic currents through Slo1. The surface-charge effect on the VSDs at the intracellular side of the channel would then counteract the stimulatory effect of PIP_2 on L_0 mediated by a distinct molecular locus (see below). According to this idea, screening of the additional negative charges provided by PIP_2, for example by Mg^{2+}, should only leave the stimulatory effect operative. The results of an illustrative experiment manipulating the intracellular Mg^{2+} concentration are depicted in Fig. 4 (A and B). Without added divalent cations, 10 µM PIP_2 caused an inhibitory positive shift of $V_{0.5}$ ($\Delta V_{0.5}$ = 19.8 ± 2.8 mV [9]) in the mutant Slo1 channel whose intracellular divalent cation sensors are disrupted (D362A:D367A:E399A:Δ894–895; Fig. 4 A, red) (Xia et al., 2002; Zhang et al., 2010). But subsequent application of 10 mM Mg^{2+} reversed the shift direction caused by PIP_2 ($\Delta V_{0.5}$ = −27.6 ± 2.8 mV [8] compared with the original condition without PIP_2) and increased currents, presumably by screening the negative surface charges provided by PIP_2 (Fig. 4 A, gray). A smaller physiological concentration of Mg^{2+} (2 mM) was also effective in reversing the "polarity" of the effect

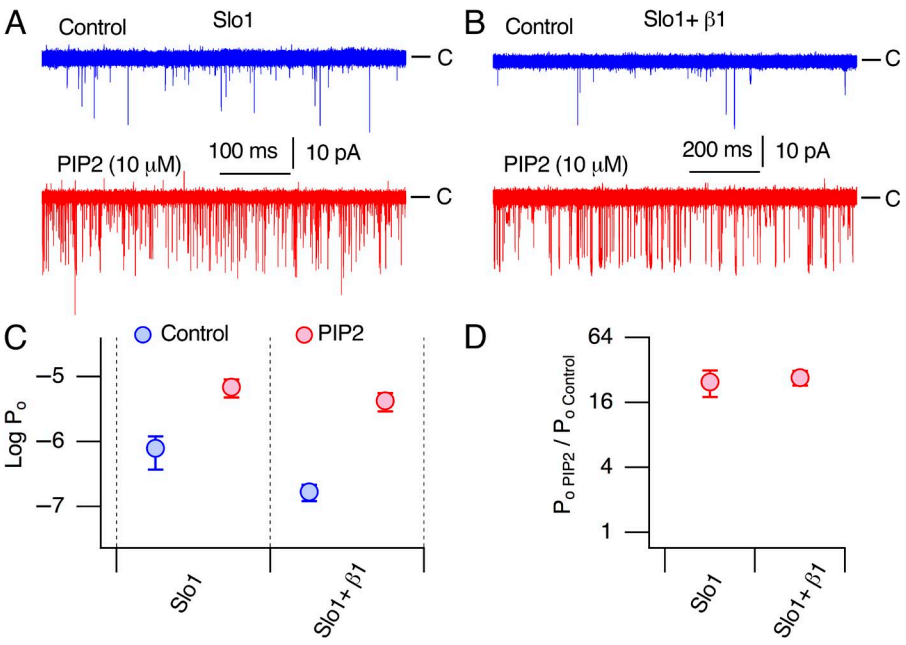

Figure 3. PIP_2 increases P_o at negative voltages without Ca^{2+}. (A) Representative single-channel openings at −120 mV of Slo1 without Ca^{2+} before and after the application of 10 µM PIP_2. In each condition, 25 data traces are shown superimposed. This patch contained ∼350 channels. (B) Representative single-channel openings at −120 mV of Slo1 + β1 without Ca^{2+} before and after the application of 10 µM PIP_2. 60 data traces are shown superimposed, and the patch contained ∼250 channels. (C) Comparison of P_o changes in Slo1 and Slo1 + β1 by 10 µM PIP_2. (D) Fractional changes in P_o by 10 µM PIP_2; n = 7 and 8 for Slo1 and Slo1 + β1, respectively. All results were obtained without Ca^{2+}. Error bars represent mean ± SEM.

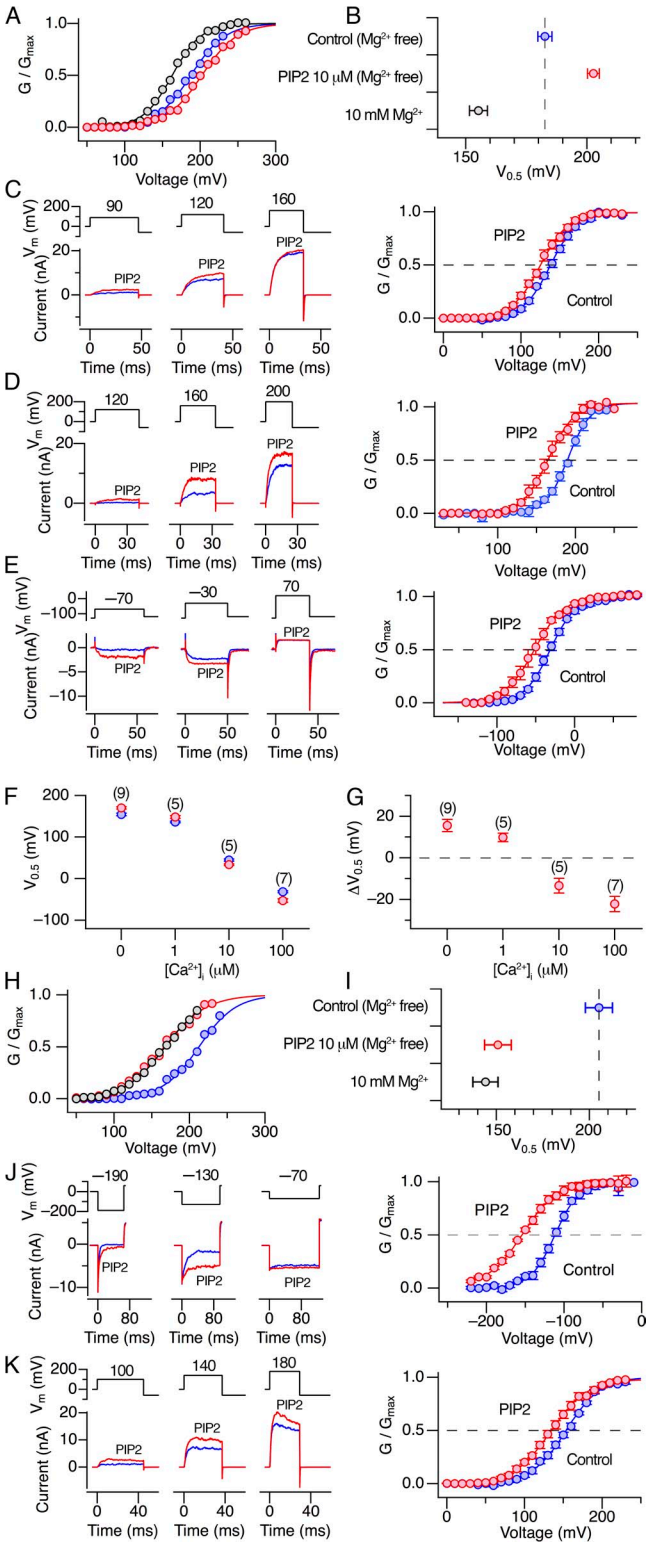

Figure 4. Manipulations of divalent cation concentrations alter the direction of the PIP_2 effect in Slo1. (A) G-V curves before (blue) and after PIP_2 addition (red), and the subsequent addition of 10 mM Mg^{2+} (black), from a representative patch expressing divalent cation–insensitive Slo1 D362A:D367A:E399A:Δ894–895 channels. (B) Changes in $V_{0.5}$ of Slo1 D362A:D367A:E399A:Δ894–895 by PIP_2 and Mg^{2+}. (C) Representative currents (left) and G-V curves from five patches (right) of wild-type Slo1 before (blue) and after (red) the application of 10 µM PIP_2 in the presence of 2 mM Mg^{2+}. (D) Representative currents (left) and G-V curves from five patches (right) containing Slo1 D362A:D367A:E399A:Δ894–895 before (blue) and after (red) the application of 10 µM PIP_2 in the presence of 100 µM Ca^{2+}. (E) Representative currents (left) and G-V curves from seven patches (right) containing wild-type Slo1 before (blue) and after (red) the application of 10 µM PIP_2 in the presence of 100 µM Ca^{2+}. (F and G) Ca^{2+} dependence of $V_{0.5}$ before (blue) and after (red) the application of 10 µM PIP_2 (F) and that of $\Delta V_{0.5}$ (G) by 10 µM PIP_2. (H) Representative currents from Slo1 D362A:D367A:E399A:Δ894–895 + β1 before (blue) and after (red) the application of 10 µM PIP_2 in the presence of 10 mM Mg^{2+}. (I) Changes in $V_{0.5}$ of Slo1 D362A:D367A:E399A:Δ894–895 + β1 by PIP_2 and Mg^{2+}; $n = 8$. (J) Representative currents (left) and G-V curves from seven patches (right) of wild-type Slo1 + β1 before (blue) and after (red) the application of 10 µM PIP_2 with 100 µM Ca^{2+} inside. (K) Representative currents (left) and G-V curves from six patches (right) containing wild-type Slo1 recorded in the outside-out configuration before (blue) and after (red) the application of 10 µM PIP_2 to the extracellular side without any added Mg^{2+} or Ca^{2+}. The $V_{0.5}$ values before and after the application of PIP_2 were 151.7 ± 1.7 mV and 137.2 ± 1.3 mV (P = 0.0021; $n = 6$). Error bars represent mean ± SEM.

of PIP_2 on Slo1 ($\Delta V_{0.5} = -12.6 \pm 2.6$ mV [5]; Fig. 4 C). In addition to Mg^{2+}, Ca^{2+} was similarly effective (Fig. 4 D). With 100 µM Ca^{2+}, a saturating concentration for the high affinity divalent cation sensors of the channel (Horrigan and Aldrich, 2002), PIP_2 enhanced currents through Slo1 D362A:D367A:E399A:Δ894–895 (Fig. 4 D; $\Delta V_{0.5} = -25.6 \pm 3.7$ mV [5]) and those through wild-type Slo1 (Fig. 4 E; $\Delta V_{0.5} = -22.2 \pm 3.7$ mV [7]) by shifting $V_{0.5}$ to the negative direction. The measurements manipulating the concentration of Ca^{2+} showed that the crossover from the stimulatory effect ($\Delta V_{0.5}$ of <0) to the inhibitory effect ($\Delta V_{0.5}$ of >0) of PIP_2 occurs around a few micromolars of [Ca^{2+}] (Fig. 4, F and G). The effectiveness of PIP_2 with 100 µM Ca^{2+} also indicates that the stimulatory action of PIP_2 does not require modulation of the high affinity Ca^{2+} sensor activation. When β1 was coexpressed, a robust stimulatory effect of PIP_2 clearly persisted with 10 mM Mg^{2+} (Slo1 D362A:D367A:E399A:Δ894–895 + β1; Fig. 4, H and I) and also with 100 µM Ca^{2+} (wild-type Slo1 + β1; Fig. 4 J). A much greater concentration of Ca^{2+} (2 mM) was required to antagonize the stimulatory effect of PIP_2 in Slo1 D362A:D367A:E399A:Δ894–895 + β1 (Fig. S4), suggesting that the stimulatory effect of PIP_2 may be mediated by a tighter interaction, potentially involving a PIP_2-binding pocket (Suh and Hille, 2008).

If excess negative charges on the intracellular membrane surface underlie the positive shift of $V_{0.5}$ by PIP_2 in Slo1, excess negative charges on the extracellular surface should produce a negative shift of $V_{0.5}$, thereby enhancing currents through Slo1. Consistent with this prediction, the application of PIP_2 to the extracellular side indeed caused a clear negative shift of $V_{0.5}$ (−14.5 ± 1.2 mV [6];

$P = 0.0021$) and increased macroscopic currents in the wild-type Slo1 channel (Fig. 4 K).

Slo1 + β1 versus Slo1 + β2 Δ2–19

The sequence alignment between β1 and β2 suggests a longer cytoplasmic N-terminal region in β2 and, even in β2 Δ2–19, the N terminus preceding TM1 is most probably longer than that in β1 (Fig. 5 A). In β2 Δ2–32, additional residues are removed and its N terminus likely contains the same number of residues as in β1 (Fig. 5 A). In Slo1 + β2 Δ2–32, PIP_2 caused a noticeable negative shift in GV ($\Delta V_{0.5} = -28.8 \pm 2.3$ mV [17]), whereas PIP_2 had essentially no effect in Slo1 + β2 Δ2–19 ($P < 10^{-7}$; but smaller than that in Slo1 + β1, $P < 10^{-6}$; Fig. 5 B). This observation suggests that the stimulatory action of PIP_2 observed in Slo1 + β2 Δ2–32 is impaired by the differences in the segment between β2 Δ2–19 and β2 Δ2–32 (residues 20–32; Fig. 5 A). This segment possesses

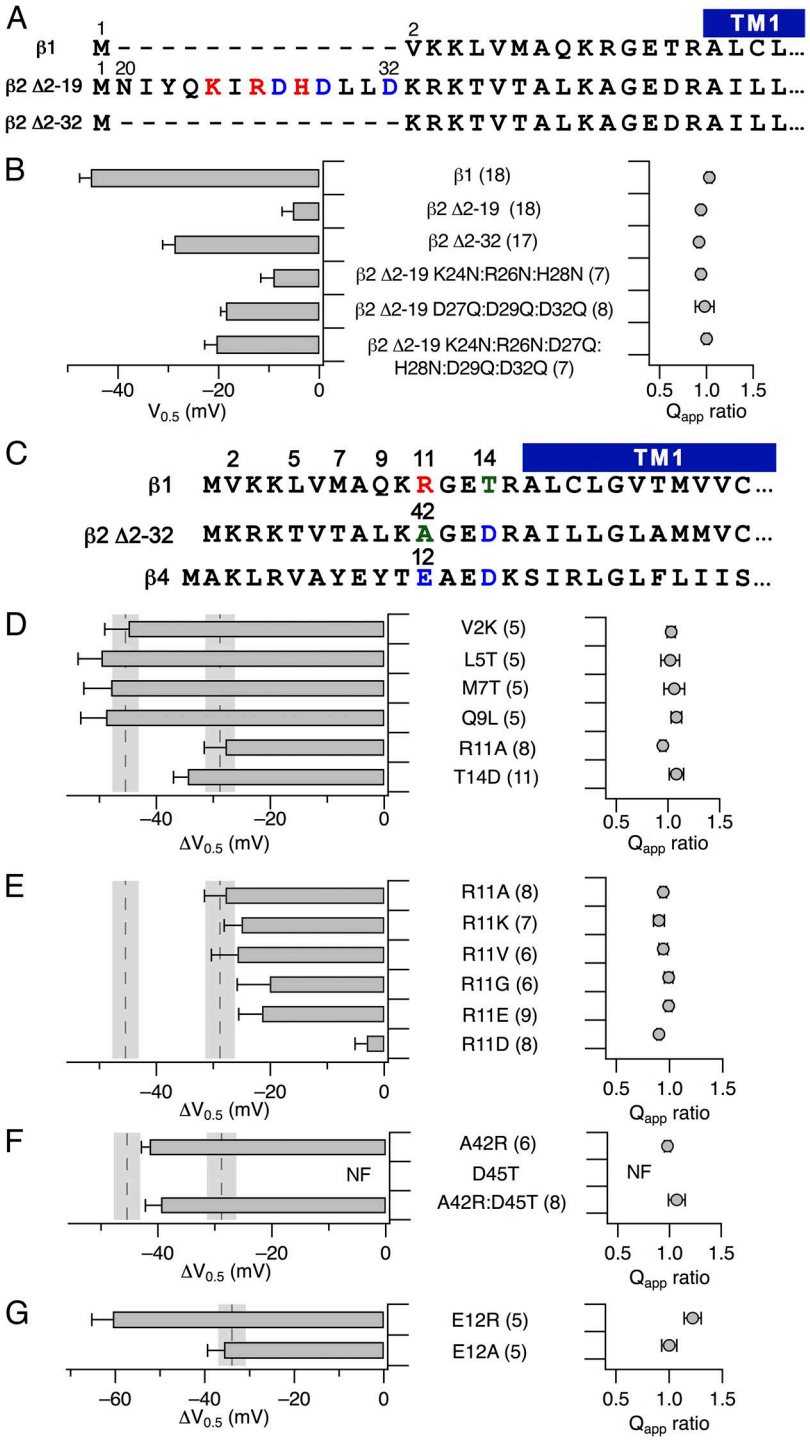

Figure 5. Critical role of the β N terminus in determining $\Delta V_{0.5}$ by PIP_2. (A) Sequence alignment of β1, β2 Δ2–19, and β2 Δ2–32 N termini. (B) Changes in G-V parameters by PIP_2 in Slo1 complexes with different β subunits. (C) Sequence alignment of β1, β2–32, and β4 N termini. (D) Changes in G-V parameters by PIP_2 in Slo1 + β1 complexes with the β1-to-β2 point mutations indicated. (E) Changes in G-V parameters by PIP_2 in Slo1 + β1 complexes with β1 mutations at position 11. (F) Changes in G-V parameters by PIP_2 in Slo1 + β2 with the β2-to-β1 point mutations indicated. (G) Changes in G-V parameters by PIP_2 in Slo1 + β4 with the β4-to-β1 (top) and β4-to-β2 (bottom) point mutations indicated. In D–F, the gray shaded areas represent the mean ± SEM of $\Delta V_{0.5}$ by PIP_2 in Slo1 + β1 (left) and Slo1 + β2 Δ2-32 (right). In G, the gray shaded area shows the mean ± SEM of $\Delta V_{0.5}$ by PIP_2 in Slo1 + β2 Δ2–32. All results were obtained without Ca^{2+}. Error bars represent mean ± SEM.

multiple positively charged residues (K24, R26, and H28 using full β2 numbering) and negatively charged residues (D27, D29, and D32), which could potentially interact with the negatively charged head group of PIP_2. Neutralization of the positively charged residues in β2 Δ2–19 (β2 Δ2–19 K24N:R26N:H28N) did not confer a greater shift of $V_{0.5}$ by PIP_2 to Slo1 + β2 Δ2–19 (Fig. 5 B). However, neutralization of the negatively charged residues (β2 Δ2–19 D27Q:D29Q:D32Q) significantly increased $\Delta V_{0.5}$ by PIP_2 to −18.6 ± 1.0 mV (8) (P = 0.00017; Fig. 5 B), indicating that there may be an electrostatic repulsion between these negatively charged residues and the PIP_2 head group. The PIP_2-induced $\Delta V_{0.5}$ in Slo1 + β2 Δ2–19 K24N:R26N:D27Q:H28N:D29Q:D32Q, in which both the positively charged residues and negatively charged residues are neutralized, was indistinguishable

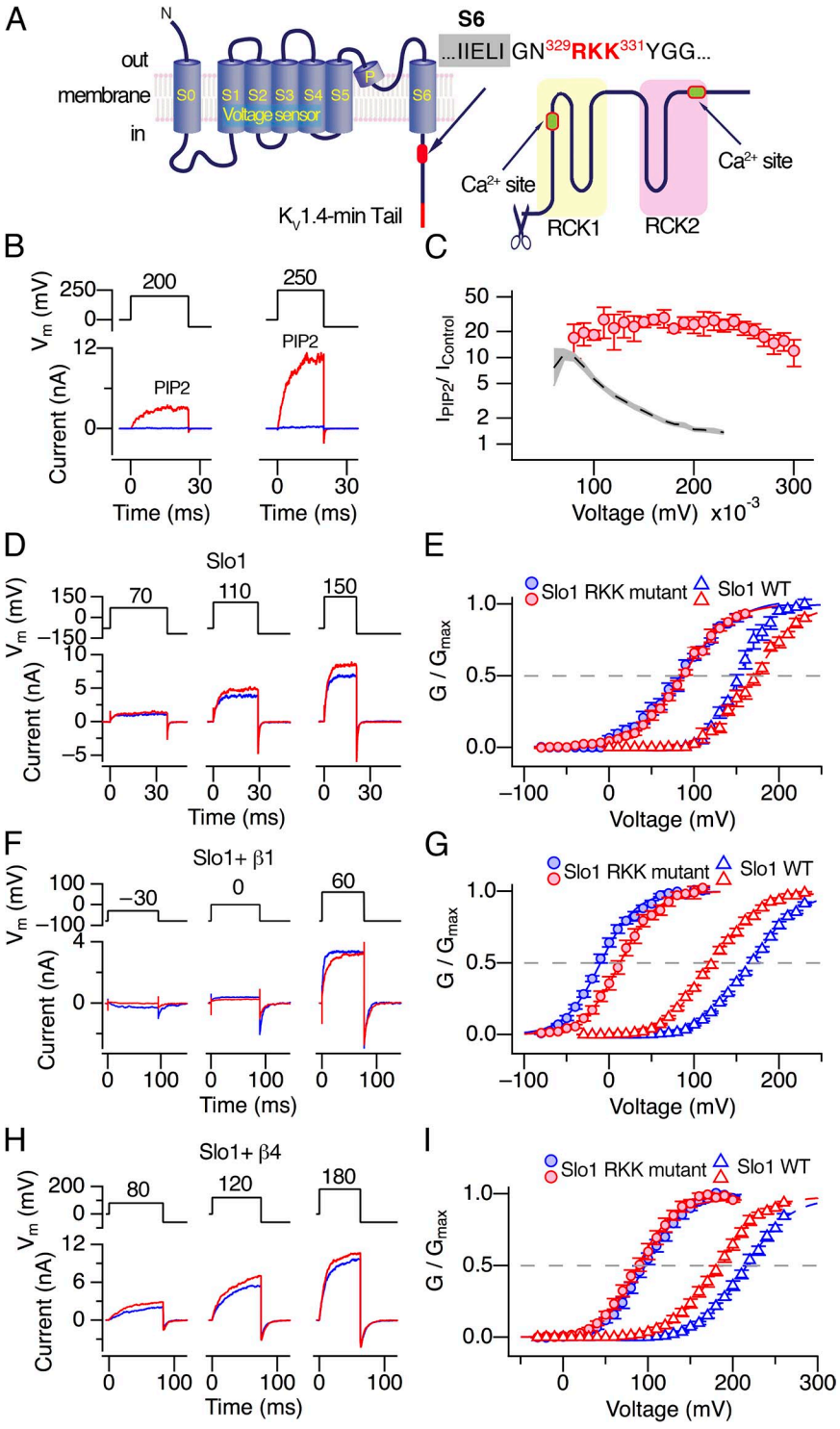

Figure 6. Roles of ^{329}RKK^{331} and the GR domain in modulation of P_o in Slo1 + β1 by PIP_2. (A) Schematic structural organization of a Slo1 subunit without the GR domain (Slo1ΔGR-Kv-minT). In Slo1ΔGR-Kv-minT, the polypeptide is truncated immediately C terminal to the sequence ^{329}RKK^{331}. The distal red segment represents the amino acids added by Budelli et al. (2013) (GVKESLG-GTDV). (B) Representative currents from Slo1ΔGR-Kv-minT + β1 before (blue) and after (red) the application of 10 µM PIP_2. (C) Fractional changes in peak outward currents at different voltages by 10 µM PIP_2 (red). The gray shaded area shows the mean ± SEM results from wild-type Slo1 + β1 for comparison. (D, F, and H) Illustrative currents through Slo1 R329A:K330A:K331A (D), Slo1 R329A:K330A:K331A + β1 (F), and Slo1 R329A:K330A:K331A + β4 (H) before (blue) and after (red) the application of 10 µM PIP_2. (E, G, and I) G-V curves of Slo1 R329A:K330A:K331A ("RKK mutant"), Slo1 R329A:K330A:K331A ("RKK mutant") + β1, and Slo1 R329A:K330A:K331A ("RKK mutant") + β4 before (blue circles) and after (red circles) the application of 10 µM PIP_2. For comparison, G-V curves from the respective wild-type Slo1 (E), Slo1 + β1 (G), and Slo1 + β4 (I) before (blue triangles) and after (red triangles) the application of 10 µM PIP_2 are also shown; n = 6–8. All results were obtained without Ca^{2+}. Error bars represent mean ± SEM.

from that in Slo1 + β2 Δ2–19 D27Q:D29Q:D32Q (P = 0.53; Fig. 5 B).

The difference in $\Delta V_{0.5}$ between Slo1 + β2 Δ2–19 and Slo1 + β2 Δ2–32 is therefore accounted for largely by the negatively charged residues D27, D29, and D32; however, the $\Delta V_{0.5}$ values in Slo1 + β2 Δ2–32 and Slo1 + β1 still differ significantly (Fig. 5 B). Similar contrasting behavior between Slo1 + β2 Δ2–19/Δ2–32 and Slo1 + β1 was observed with the stimulatory effect of the omega-3 fatty acid docosahexaenoic acid (DHA), and the N-terminal residues in β1 and β2 Δ2–32 (Fig. 5 C) were found to be critical (Hoshi et al., 2013b). We thus examined if the N termini of β1 and β2 Δ2–32 also contributed to the difference in PIP_2-induced $\Delta V_{0.5}$ in Slo1 + β1 and Slo1 + β2 Δ2–32 by introducing β1-to-β2 single-residue mutations to β1 (Figs. 5, C and D, and S5). The β1-to-β2 mutations V2K, L5T, M7T, and Q9L in the β1 background failed to alter $\Delta V_{0.5}$ by PIP_2. The β1-to-β2 mutations R11A and T14D in β1 diminished the $\Delta V_{0.5}$ of the resulting Slo1 + β1 complexes by PIP_2 from −45 mV to −27.9 ± 3.6 mV (8) and −34.5 ± 2.5 mV (11), respectively, which were indistinguishable from that observed in Slo1 + β1 Δ2–32 (P = 0.80 and 0.09, respectively). A higher bulk concentration of PIP_2 (30 µM) did not produce a greater change (not depicted). Mutation of R11 in β1 to other amino acids, neutral and charged including Lys, also noticeably diminished the $\Delta V_{0.5}$ by PIP_2 (Fig. 5 E). In particular, the mutation R11D essentially eliminated the effect of PIP_2 on Slo1 + β1 (Fig. 5 E); the reason for this particularly large effect of R11D is unclear.

The critical nature of Arg at position 11 in β1 is further suggested by the converse β2-to-β1 mutation A42R in the β2 background in which Ala at position 42 of β2, equivalent to position 11 in β1 (Fig. 5 F), is substituted with Arg as found in β1. This point mutation conferred a greater $\Delta V_{0.5}$ by PIP_2 to Slo1 + β2 Δ2–32 (−41.5 ± 1.4 mV [6]), indistinguishable from that found in Slo1 + β1 (P = 0.38). The mutation β2 D45T, the β2-to-β1 mutation at position 45 in β2, equivalent to position 14 in β1 (Fig. 5 C), did not produce a functional β2 subunit. The double mutant β2 A42R:D45T was functional and the $\Delta V_{0.5}$ by PIP_2 in Slo1 + β2 A42R:D45T did not differ from that in Slo1 + β1 A42R (Fig. 5 F; P = 0.35). Mutation of charged Glu at position 12 in β4, equivalent to position 11 in β1, to Arg (E12R) as in β1 (Fig. 5 C), enhanced the $\Delta V_{0.5}$ in the Slo1 + β4 from −34 mV to −60.6 ± 4.7 mV (5), which is even greater than that in Slo1 + β1 (Fig. 5 G; P = 0.007). In contrast, the β4-to-β2 mutation β4 E12A did not alter $\Delta V_{0.5}$ by PIP_2 in Slo1 + β4 (Fig. 5 G; P = 0.78). Collectively, the presence of Arg at positions equivalent to position 11 in β1 clearly plays a pivotal role in determining $\Delta V_{0.5}$ by PIP_2 in Slo1 + β complexes.

Essential molecular loci

Two areas of the Slo1 channel have been implicated in the stimulatory effects of PIP_2 in earlier studies: ^{329}RKK^{331} immediately C terminal to S6 but N terminal to the RCK1 segment (Vaithianathan et al., 2008), and the ^{366}KDRDD^{370} loop in the RCK1 Ca^{2+}-sensor area in the GR domain (Tang et al., 2014). The contribution of the GR domain including the RCK1 Ca^{2+}-sensor area and its vicinity to the PIP_2-mediated regulation was assessed using the truncated Slo1 channel without the GR domain but with the ^{329}RKK^{331} sequence intact (Slo1ΔGR-Kv-minT; Budelli et al., 2013; Fig. 6 A). The voltage dependence of Slo1ΔGR-Kv-minT + β1 was shifted markedly to the positive direction, and an accurate determination of its G-V was not practical. However, PIP_2 unmistakably increased currents through Slo1ΔGR-Kv-minT + β1 (Fig. 6, B and C); the GR domain is not required for the stimulatory action of PIP_2 on the Slo1 + β1 complex. Furthermore, PIP_2 also remained effective in activating Slo1 D362A:D367A:E399A:Δ894–895 + β1, in which both the high affinity and low affinity divalent cation sensors are impaired (Xia et al., 2002; Zhang et al., 2010) ($\Delta V_{0.5}$ = −53.3 ± 5.8 mV [14]; P = 0.16 compared with WT Slo1 + β1; Fig. S6).

The sequence ^{329}RKK^{331} immediately C terminal to S6 has also been implicated in the action of PIP_2 (Vaithianathan et al., 2008). The mutation Slo1 R329A:K330A:K331A was reported to diminish the stimulatory effect of PIP_2 when measured with an intermediate $[Ca^{2+}]_i$ (0.3 µM) (Vaithianathan et al., 2008). Our measurements without Ca^{2+} with Slo1 R329A:K330A:K331A + β1 revealed that the mutation drastically shifted the voltage dependence to the negative direction (Fig. 6, F and G). The application of PIP_2 failed to enhance currents through Slo1 R329A:K330A:K331A + β1 and caused a positive shift of $V_{0.5}$ ($\Delta V_{0.5}$ = 22.9 ± 5.1 mV [6]; $P < 10^{-4}$ compared with Slo1 + β1; Fig. 6, F and G). In Slo1 R329A:K330A:K331A (Fig. 6, D and E) and Slo1 R329A:K330A:K331A + β4 (Fig. 6, H and I), PIP_2 failed to alter $V_{0.5}$ (P = 0.64 and 0.31, respectively).

DISCUSSION

Slo1 BK channels are widely expressed in different tissues and play important roles in numerous physiological phenomena (Salkoff et al., 2006; Hoshi et al., 2013a). Two of the important factors contributing to the functional versatility of Slo1 BK channels are tissue-dependent inclusion of auxiliary subunits and modulation of their gating by different signaling molecules (Salkoff et al., 2006; Hou et al., 2009; Hoshi et al., 2013a). Our study here demonstrates that brain-derived PIP_2, most probably with stearic and arachidonic tails (Balla, 2013), regulates Slo1 BK channels in a subunit composition–dependent manner through two distinct biophysical mechanisms. At the voltages where VSD activation and G/G_{max} are appreciable (e.g., >0.05), PIP_2 inhibits currents through Slo1 and Slo1 + γ1 but markedly increases currents

through Slo1 + β1 and to a lesser extent those through Slo1 + β4.

The inhibitory effect of PIP_2 on macroscopic currents through Slo1 in patches taken from human embryonic kidney cells and *Xenopus* oocytes is in contrast with the results obtained by Vaithianathan et al. (2008), who showed a noticeable increase in P_o of Slo1 (without any auxiliary subunit) heterologously expressed in *Xenopus* oocytes and also of native Slo1 in skeletal muscle cells. Using Slo1 without auxiliary subunits expressed in *Xenopus* oocytes, Tang et al. (2014) also observed a current-enhancing effect of PIP_2 after pretreatment with the phosphoinositide 3-kinase inhibitor wortmannin (25 µM for ≥2 h). The exact reasons for the divergent observations remain unclear. It is possible that PIP_2 exerts multiple actions, some of which are observed preferentially under different experimental conditions. Perhaps seemingly subtle differences in cell culturing/preparation methods, potentially affecting the membrane lipid composition (Epand, 2008), may also underlie the contrasting observations.

Our electrophysiological measurements manipulating membrane potential and $[Ca^{2+}]_i$ to isolate specific aspects of gating of the Slo1 BK channel complex suggest that the application of exogenous brain-derived PIP_2 induces two separate effects with different divalent cation sensitivities depending on the subunit composition. The effect of PIP_2 observed in both Slo1 and Slo1 + β1, and most probably in all others, is to bias the equilibrium of the ion conduction gate, L_0 in the HA model (Horrigan and Aldrich, 2002), toward the open state. Such a change shifts $V_{0.5}$ to the negative direction as observed in Slo1 + β1, Slo1 + β2 Δ2–32, and Slo1 + β4. This increase in L_0 is probably mediated by the binding of PIP_2 to the sequence ^{329}RKK^{331} immediately C terminal to S6 because the Slo1 mutation R329A:K330A:K331A (Vaithianathan et al., 2008) appears to disrupt the stimulatory effect of PIP_2 on Slo1 + β1. It should be noted, however, that the mutation itself without any exogenous PIP_2 strikingly shifts the voltage dependence of activation to the negative direction, and some interpretational uncertainty exists. The interaction between the sequence ^{329}RKK^{331} and the negative charges of brain-derived PIP_2 is stabilized by its long 18- and 20-carbon tail groups, most probably in the membrane, causing a near irreversible action of PIP_2. In contrast, diC8 with short tails produces a smaller and more reversible effect. Quantum and molecular dynamics simulations suggest that Ca^{2+} interacts with the negative charges of PIP_2 more closely than Mg^{2+} (Slochower et al., 2013). Consistent with the simulation results, we find that 2 mM Ca^{2+} disrupts the stimulatory effect of PIP_2 on P_o of Slo1 + β1, but the increase persists with 10 mM Mg^{2+}. Besides the sequence ^{329}RKK^{331}, the RCK1 Ca^{2+} sensor in the GR domain has been implicated in the stimulatory action of PIP_2 (Tang et al., 2014). However, an essential role of the GR domain may be excluded, at least in our experimental conditions, because the truncated Slo1 channel without the GR domain can be robustly stimulated by PIP_2 when coexpressed with β1.

Multiple studies suggest that the S6-RCK1 linker segment containing the sequence ^{329}RKK^{331} is a critical structural determinant of Slo1 gating. This segment has been suggested to function as a passive mechanical spring affecting the overall voltage dependence of channel activation (Niu et al., 2004). The mutation of ^{329}RKK^{331}, which alters the response to PIP_2 (Vaithianathan et al., 2008) (Fig. 6), produces a very large shift in voltage dependence of activation (Fig. 6). Furthermore, the segment also regulates the sensitivity of the channel to so-called BK openers such as the dehydroabietic acid derivative Cym04 and NS1619, both of which increase L_0 (Gessner et al., 2012) as found for PIP_2. The interaction of PIP_2 with the sequence ^{329}RKK^{331} may facilitate the rotational movement of the S6 side chains that is speculated to accompany the opening of the ion conduction gate (Chen et al., 2014). How this may occur remains an open question.

In Slo1, but not in those with β subunits, PIP_2 inhibits ionic currents at the voltages where VSD activation is appreciable by providing additional negative surface charges on the intracellular surface of the membrane, as suggested by the results of our experiments designed to screen the negative surface charges provided by PIP_2 with Mg^{2+} (Fig. 4). 2 mM Mg^{2+} or 100 µM Ca^{2+} is sufficient to antagonize this surface charge effect. Assuming that the transmembrane segments of Slo1 are organized like those in Kv1.2/2.1 (Long et al., 2007), one VSD in Slo1 is separated from an adjacent VSD by membrane lipids. We postulate that PIP_2 molecules may position in this cleft area between two neighboring VSDs and provide additional negative charges that could be sensed by the VSDs, thus altering the voltage-sensor equilibrium of the channel. Extracellular disulfide cross-linking studies suggest that the two transmembrane segments of β subunits occupy this same area between the adjacent VSDs (Wu et al., 2009, 2013; Morera et al., 2012; Liu et al., 2015). We propose that this positioning of β subunits prevents the negative charges of PIP_2 molecules from closely approaching the VSDs while allowing for the interaction of PIP_2 with the sequence ^{329}RKK^{331} to increase L_0. The three-dimensional structural location of the sequence ^{329}RKK^{331} within Slo1 is unknown; however, we speculate that these residues may be situated near the radial periphery of the channel such that PIP_2 has a ready access. Unlike β subunits with two membrane-spanning segments, γ1 with one membrane-spanning segment (Yan and Aldrich, 2010) may allow PIP_2 to approach the VSDs; currents through Slo1 + γ1 at positive voltages are inhibited by PIP_2 applied to the intracellular side as in Slo1. One unexpected set of findings concerns Slo1 R329A:K330A:K331A, in which the sequence

^{329}RKK^{331} is neutralized. Without any β or γ subunit, PIP_2 was expected to cause a positive shift in voltage dependence of activation in Slo1 R329A:K330A:K331A, but the observed shift is negligible. Additionally, in Slo1 R329A:K330A:K331A + β1, in which juxtaposition of PIP_2 and the VSDs was expected to be impaired by β1, PIP_2 induces a positive shift. In contrast, the results from Slo1 R329A:K330A:K331A + β4 are in line with our expectation. Some of the results using Slo1 R329A:K330A:K331A are thus difficult to interpret in part because of the severe basal phenotype of this mutant.

In Slo1 + β complexes, the β N terminus plays a critical role in determining the extent of current enhancement by PIP_2. Our mutagenesis results show that three negatively charged Asp residues in the β2 N terminus at positions 27, 29, and 32 impair the electrophysiological response of the channel complex to PIP_2. We propose that an electrostatic repulsion between these β2 Asp residues and the PIP_2 head group may exist, interfering with the interaction of the PIP_2 head group with the probable effector sequence ^{329}RKK^{331} in Slo1. In addition to the Asp residues in the β2 N terminus, Arg at position 11 of β1 is also critical. Even a charge-conserved substitution with Lys at this position markedly diminishes the response of the channel complex to PIP_2. At the extracellular side, β TM1 is probably 2 to 3 nm away from Slo1 S6 (Wu et al., 2009, 2013; Liu et al., 2010, 2015), and the β N terminus with ∼15 residues could position itself near the cytoplasmic end of S6 or the S6-RCK1 segment. Asp at position 45 in β2, equivalent to position 14 in β1, has been suggested to interact with the residues near the RCK1 Ca^{2+} sensor (Hou et al., 2013). The importance of Arg at position 11 was also suggested for the stimulatory effect of DHA on Slo1 + β1 mediated by an increase in L_0 (Hoshi et al., 2013b). Although both DHA and PIP_2 increase L_0 in Slo1 + β1, the mutation R11K in β1 preserves the wild-type–like response to DHA (Hoshi et al., 2013b) but not to PIP_2. Thus, the structural interactions involving Arg at position 11 in β1 required for the effects of DHA and PIP_2 appear to be different.

PIP_2 regulates numerous proteins including ion channels with different affinities (Suh and Hille, 2008). Some channels have very high affinities for PIP_2, which essentially acts as a cofactor necessary for proper functionality (Suh and Hille, 2008). For others, PIP_2 acts as a dynamic reversible modulator of their functions (Suh and Hille, 2008). In Slo1 BK channels, PIP_2 has multiple sites of action, targeting different functional aspects: the number of channels available to open (Tang et al., 2014), Ca^{2+}-dependent activation (Tang et al., 2014), voltage-dependent activation (this study), and intrinsic gating of the ion conduction gate (this study). The finding that the PIP_2-mediated modulation depends strongly on the auxiliary subunit composition suggests that PIP_2 regulates Slo1 BK channels in a tissue-dependent manner, further increasing the functional versatility of the channels.

We thank Drs. Y. Ramu and Z. Lu for assistance with *Xenopus* oocytes.

This work was supported by the public in part through grants from the National Institutes of Health (R01GM057654), German Research Foundation (DFG FOR 1738, HE2993/8), and the Key Project of Shanghai Science and Technology Commission (contract no. 11JC1406400).

The authors declare no competing financial interests.

Richard W. Aldrich served as editor.

Submitted: 14 January 2015
Accepted: 9 March 2015

REFERENCES

Almassy, J., and T. Begenisich. 2012. The LRRC26 protein selectively alters the efficacy of BK channel activators. *Mol. Pharmacol.* 81:21–30. http://dx.doi.org/10.1124/mol.111.075234

Balla, T. 2013. Phosphoinositides: Tiny lipids with giant impact on cell regulation. *Physiol. Rev.* 93:1019–1137. http://dx.doi.org/10.1152/physrev.00028.2012

Behrens, R., A. Nolting, F. Reimann, M. Schwarz, R. Waldschütz, and O. Pongs. 2000. hKCNMB3 and hKCNMB4, cloning and characterization of two members of the large-conductance calcium-activated potassium channel β subunit family. *FEBS Lett.* 474:99–106. http://dx.doi.org/10.1016/S0014-5793(00)01584-2

Brenner, R., T.J. Jegla, A. Wickenden, Y. Liu, and R.W. Aldrich. 2000. Cloning and functional characterization of novel large conductance calcium-activated potassium channel β subunits, hKCNMB3 and hKCNMB4. *J. Biol. Chem.* 275:6453–6461. http://dx.doi.org/10.1074/jbc.275.9.6453

Budelli, G., Y. Geng, A. Butler, K.L. Magleby, and L. Salkoff. 2013. Properties of Slo1 K^+ channels with and without the gating ring. *Proc. Natl. Acad. Sci. USA.* 110:16657–16662. http://dx.doi.org/10.1073/pnas.1313433110

Chen, X., J. Yan, and R.W. Aldrich. 2014. BK channel opening involves side-chain reorientation of multiple deep-pore residues. *Proc. Natl. Acad. Sci. USA.* 111:E79–E88. http://dx.doi.org/10.1073/pnas.1321697111

Dopico, A.M., and A.N. Bukiya. 2014. Lipid regulation of BK channel function. *Front Physiol.* 5:312. http://dx.doi.org/10.3389/fphys.2014.00312

Epand, R.M. 2008. Proteins and cholesterol-rich domains. *Biochim. Biophys. Acta.* 1778:1576–1582. http://dx.doi.org/10.1016/j.bbamem.2008.03.016

Evanson, K.W., J.P. Bannister, M.D. Leo, and J.H. Jaggar. 2014. LRRC26 is a functional BK channel auxiliary γ subunit in arterial smooth muscle cells. *Circ. Res.* 115:423–431. http://dx.doi.org/10.1161/CIRCRESAHA.115.303407

Flynn, G.E., and W.N. Zagotta. 2011. Molecular mechanism underlying phosphatidylinositol 4,5-bisphosphate-induced inhibition of SpIH channels. *J. Biol. Chem.* 286:15535–15542. http://dx.doi.org/10.1074/jbc.M110.214650

Gamper, N., and M.S. Shapiro. 2007. Regulation of ion transport proteins by membrane phosphoinositides. *Nat. Rev. Neurosci.* 8:921–934. http://dx.doi.org/10.1038/nrn2257

Gessner, G., Y.M. Cui, Y. Otani, T. Ohwada, M. Soom, T. Hoshi, and S.H. Heinemann. 2012. Molecular mechanism of pharmacological activation of BK channels. *Proc. Natl. Acad. Sci. USA.* 109:3552–3557. http://dx.doi.org/10.1073/pnas.1114321109

Hansen, S.B., X. Tao, and R. MacKinnon. 2011. Structural basis of PIP_2 activation of the classical inward rectifier K^+ channel Kir2.2. *Nature.* 477:495–498. http://dx.doi.org/10.1038/nature10370

Hite, R.K., J.A. Butterwick, and R. MacKinnon. 2014. Phosphatidic acid modulation of Kv channel voltage sensor function. *eLife.* 3:e04366. http://dx.doi.org/10.7554/eLife.04366

Horrigan, F.T., and R.W. Aldrich. 2002. Coupling between voltage sensor activation, Ca^{2+} binding and channel opening in large conductance (BK) potassium channels. *J. Gen. Physiol.* 120:267–305. http://dx.doi.org/10.1085/jgp.20028605

Horrigan, F.T., S.H. Heinemann, and T. Hoshi. 2005. Heme regulates allosteric activation of the Slo1 BK channel. *J. Gen. Physiol.* 126:7–21. http://dx.doi.org/10.1085/jgp.200509262

Hoshi, T., A. Pantazis, and R. Olcese. 2013a. Transduction of voltage and Ca^{2+} signals by Slo1 BK channels. *Physiology (Bethesda).* 28:172–189. http://dx.doi.org/10.1152/physiol.00055.2012

Hoshi, T., Y. Tian, R. Xu, S.H. Heinemann, and S. Hou. 2013b. Mechanism of the modulation of BK potassium channel complexes with different auxiliary subunit compositions by the omega-3 fatty acid DHA. *Proc. Natl. Acad. Sci. USA.* 110:4822–4827. http://dx.doi.org/10.1073/pnas.1222003110

Hoshi, T., B. Wissuwa, Y. Tian, N. Tajima, R. Xu, M. Bauer, S.H. Heinemann, and S. Hou. 2013c. Omega-3 fatty acids lower blood pressure by directly activating large-conductance Ca^{2+}-dependent K^+ channels. *Proc. Natl. Acad. Sci. USA.* 110:4816–4821. http://dx.doi.org/10.1073/pnas.1221997110

Hou, P., W. Zeng, G. Gan, C. Lv, X. Guo, Z. Zhang, H. Liu, Y. Wu, J. Yao, A.D. Wei, et al. 2013. Inter-α/β subunits coupling mediating pre-inactivation and augmented activation of BK_{Ca}(β2). *Sci Rep.* 3:1666.

Hou, S., S.H. Heinemann, and T. Hoshi. 2009. Modulation of BK_{Ca} channel gating by endogenous signaling molecules. *Physiology (Bethesda).* 24:26–35. http://dx.doi.org/10.1152/physiol.00032.2008

Knaus, H.G., A. Eberhart, G.J. Kaczorowski, and M.L. Garcia. 1994a. Covalent attachment of charybdotoxin to the β-subunit of the high conductance Ca^{2+}-activated K^+ channel. Identification of the site of incorporation and implications for channel topology. *J. Biol. Chem.* 269:23336–23341.

Knaus, H.G., M. Garcia-Calvo, G.J. Kaczorowski, and M.L. Garcia. 1994b. Subunit composition of the high conductance calcium-activated potassium channel from smooth muscle, a representative of the mSlo and slowpoke family of potassium channels. *J. Biol. Chem.* 269:3921–3924.

Liu, G., X. Niu, R.S. Wu, N. Chudasama, Y. Yao, X. Jin, R. Weinberg, S.I. Zakharov, H. Motoike, S.O. Marx, and A. Karlin. 2010. Location of modulatory β subunits in BK potassium channels. *J. Gen. Physiol.* 135:449–459.

Liu, G., S.I. Zakharov, Y. Yao, S.O. Marx, and A. Karlin. 2015. Positions of the cytoplasmic end of BK α S0 helix relative to S1–S6 and of β1 TM1 and TM2 relative to S0–S6. *J. Gen. Physiol.* 145:185–199. http://dx.doi.org/10.1085/jgp.201411337

Long, S.B., X. Tao, E.B. Campbell, and R. MacKinnon. 2007. Atomic structure of a voltage-dependent K^+ channel in a lipid membrane-like environment. *Nature.* 450:376–382. http://dx.doi.org/10.1038/nature06265

Morera, F.J., A. Alioua, P. Kundu, M. Salazar, C. Gonzalez, A.D. Martinez, E. Stefani, L. Toro, and R. Latorre. 2012. The first transmembrane domain (TM1) of β2-subunit binds to the transmembrane domain S1 of α-subunit in BK potassium channels. *FEBS Lett.* 586:2287–2293. http://dx.doi.org/10.1016/j.febslet.2012.05.066

Nelson, M.T., and A.D. Bonev. 2004. The β1 subunit of the Ca^{2+}-sensitive K^+ channel protects against hypertension. *J. Clin. Invest.* 113:955–957. http://dx.doi.org/10.1172/JCI21388

Niu, X., X. Qian, and K.L. Magleby. 2004. Linker-gating ring complex as passive spring and Ca^{2+}-dependent machine for a voltage- and Ca^{2+}-activated potassium channel. *Neuron.* 42:745–756. http://dx.doi.org/10.1016/j.neuron.2004.05.001

Pian, P., A. Bucchi, R.B. Robinson, and S.A. Siegelbaum. 2006. Regulation of gating and rundown of HCN hyperpolarization-activated channels by exogenous and endogenous PIP_2. *J. Gen. Physiol.* 128:593–604. http://dx.doi.org/10.1085/jgp.200609648

Ramu, Y., Y. Xu, and Z. Lu. 2006. Enzymatic activation of voltage-gated potassium channels. *Nature.* 442:696–699. http://dx.doi.org/10.1038/nature04880

Rittenhouse, A.R. 2008. PIP_2 PIP_2 hooray for maxi K^+. *J. Gen. Physiol.* 132:5–8. http://dx.doi.org/10.1085/jgp.200810053

Salkoff, L., A. Butler, G. Ferreira, C. Santi, and A. Wei. 2006. High-conductance potassium channels of the SLO family. *Nat. Rev. Neurosci.* 7:921–931. http://dx.doi.org/10.1038/nrn1992

Slochower, D.R., P.J. Huwe, R. Radhakrishnan, and P.A. Janmey. 2013. Quantum and all-atom molecular dynamics simulations of protonation and divalent ion binding to phosphatidylinositol 4,5-bisphosphate (PIP_2). *J. Phys. Chem. B.* 117:8322–8329. http://dx.doi.org/10.1021/jp401414y

Suh, B.C., and B. Hille. 2008. PIP_2 is a necessary cofactor for ion channel function: How and why? *Annu Rev Biophys.* 37: 175–195. http://dx.doi.org/10.1146/annurev.biophys.37.032807.125859

Tang, Q.Y., Z. Zhang, X.Y. Meng, M. Cui, and D.E. Logothetis. 2014. Structural determinants of phosphatidylinositol 4,5-bisphosphate (PIP_2) regulation of BK channel activity through the RCK1 Ca^{2+} coordination site. *J. Biol. Chem.* 289:18860–18872. http://dx.doi.org/10.1074/jbc.M113.538033

Uebele, V.N., A. Lagrutta, T. Wade, D.J. Figueroa, Y. Liu, E. McKenna, C.P. Austin, P.B. Bennett, and R. Swanson. 2000. Cloning and functional expression of two families of β-subunits of the large conductance calcium-activated K^+ channel. *J. Biol. Chem.* 275:23211–23218. http://dx.doi.org/10.1074/jbc.M910187199

Vaithianathan, T., A. Bukiya, J. Liu, P. Liu, M. Asuncion-Chin, Z. Fan, and A. Dopico. 2008. Direct regulation of BK channels by phosphatidylinositol 4,5-bisphosphate as a novel signaling pathway. *J. Gen. Physiol.* 132:13–28. http://dx.doi.org/10.1085/jgp.200709913

Wallner, M., P. Meera, and L. Toro. 1999. Molecular basis of fast inactivation in voltage and Ca^{2+}-activated K^+ channels: A transmembrane β-subunit homolog. *Proc. Natl. Acad. Sci. USA.* 96:4137–4142. http://dx.doi.org/10.1073/pnas.96.7.4137

Wang, Y.H., D.R. Slochower, and P.A. Janmey. 2014. Counterion-mediated cluster formation by polyphosphoinositides. *Chem. Phys. Lipids.* 182:38–51. http://dx.doi.org/10.1016/j.chemphyslip.2014.01.001

Wang, Y.W., J.P. Ding, X.M. Xia, and C.J. Lingle. 2002. Consequences of the stoichiometry of *Slo1* α and auxiliary β subunits on functional properties of large-conductance Ca^{2+}-activated K^+ channels. *J. Neurosci.* 22:1550–1561.

Womack, K.B., S.E. Gordon, F. He, T.G. Wensel, C.C. Lu, and D.W. Hilgemann. 2000. Do phosphatidylinositides modulate vertebrate phototransduction? *J. Neurosci.* 20:2792–2799.

Wu, R.S., N. Chudasama, S.I. Zakharov, D. Doshi, H. Motoike, G. Liu, Y. Yao, X. Niu, S.X. Deng, D.W. Landry, et al. 2009. Location of the β4 transmembrane helices in the BK potassium channel. *J. Neurosci.* 29:8321–8328. http://dx.doi.org/10.1523/JNEUROSCI.6191-08.2009

Wu, R.S., G. Liu, S.I. Zakharov, N. Chudasama, H. Motoike, A. Karlin, and S.O. Marx. 2013. Positions of β2 and β3 subunits in the large-conductance calcium- and voltage-activated BK potassium channel. *J. Gen. Physiol.* 141:105–117. http://dx.doi.org/10.1085/jgp.201210891

Xia, X.M., J.P. Ding, and C.J. Lingle. 1999. Molecular basis for the inactivation of Ca^{2+}- and voltage-dependent BK channels in adrenal chromaffin cells and rat insulinoma tumor cells. *J. Neurosci.* 19:5255–5264.

Xia, X.M., X. Zeng, and C.J. Lingle. 2002. Multiple regulatory sites in large-conductance calcium-activated potassium channels. *Nature.* 418:880–884. http://dx.doi.org/10.1038/nature00956

Xia, X.M., J.P. Ding, and C.J. Lingle. 2003. Inactivation of BK channels by the NH_2 terminus of the β2 auxiliary subunit: An essential role of a terminal peptide segment of three hydrophobic residues. *J. Gen. Physiol.* 121:125–148. http://dx.doi.org/10.1085/jgp.20028667

Xu, Y., Y. Ramu, and Z. Lu. 2008. Removal of phospho-head groups of membrane lipids immobilizes voltage sensors of K^+ channels. *Nature.* 451:826–829. http://dx.doi.org/10.1038/nature06618

Yan, J., and R.W. Aldrich. 2010. LRRC26 auxiliary protein allows BK channel activation at resting voltage without calcium. *Nature.* 466:513–516. http://dx.doi.org/10.1038/nature09162

Yan, J., and R.W. Aldrich. 2012. BK potassium channel modulation by leucine-rich repeat-containing proteins. *Proc. Natl. Acad. Sci. USA.* 109:7917–7922. http://dx.doi.org/10.1073/pnas.1205435109

Yang, C., X.H. Zeng, Y. Zhou, X.M. Xia, and C.J. Lingle. 2011. LRRC52 (leucine-rich-repeat-containing protein 52), a testis-specific auxiliary subunit of the alkalization-activated Slo3 channel. *Proc. Natl. Acad. Sci. USA.* 108:19419–19424. http://dx.doi.org/10.1073/pnas.1111104108

Zhang, G., R. Xu, S.H. Heinemann, and T. Hoshi. 2006. Cysteine oxidation and rundown of large-conductance Ca^{2+}-dependent K^+ channels. *Biochem. Biophys. Res. Commun.* 342:1389–1395. http://dx.doi.org/10.1016/j.bbrc.2006.02.079

Zhang, G., S.Y. Huang, J. Yang, J. Shi, X. Yang, A. Moller, X. Zou, and J. Cui. 2010. Ion sensing in the RCK1 domain of BK channels. *Proc. Natl. Acad. Sci. USA.* 107:18700–18705. http://dx.doi.org/10.1073/pnas.1010124107